Calcium Ion Binding between Lipid Bilayers: The Four-Component System of Phosphatidylserine, Phosphatidylcholine, Calcium Chloride, and Water†

Gerald W. Feigenson
Section of Biochemistry, Molecular and Cell Biology, Clark Hall, Cornell University, Ithaca, New York 14853
Received July 11, 1988; Revised Manuscript Received September 15, 1988

ABSTRACT: Ca^{2+} binding between lamellae of phosphatidylserine (PS) and phosphatidylcholine (PC) gives rise to a rigid phase of $Ca(PS)_2$. When aqueous Ca^{2+}, hydrated PS/PC, and $Ca(PS)_2$ coexist at equilibrium, the aqueous Ca^{2+} concentration is invariant and is characteristic of the PS/PC ratio. This characteristic Ca^{2+} concentration is 0.040 μM for palmitoyloleoylphosphatidylserine without PC and increases as the inverse square of the PS mole fraction at high PS concentration (Raoult's law) and as the inverse square of the PS mole fraction multiplied by a constant at low PS concentration (Henry's law). For example, for palmitoyloleoylphosphatidylserine/palmitoyloleoylphosphatidylcholine = 0.6/0.4 or 0.2/0.8, this characteristic Ca^{2+} concentration is about 0.1 or about 6 μM, respectively. These observations at constant temperature are summarized in a quaternary phase diagram for the four-component system $CaCl_2$/PS/PC/water.

Binding of Ca^{2+} between phospholipid bilayers might be a good model for one step in Ca^{2+}-induced fusion of biological membranes (Ohnishi & Ito, 1974; Koter et al., 1978; Portis et al., 1979; Liao & Prestegard, 1980; Ekerdt et al., 1981; Ekerdt & Papahadjopoulos, 1982; Nir et al., 1983; Morris et al., 1983; Ohki, 1984; Leventis et al., 1986). We have previously studied a chemically simple system of phosphatidylserine (PS),[1] Ca^{2+}, and H_2O and found that a phase of $Ca(PS)_2$ forms under the physiologically interesting conditions of excess H_2O and submicromolar Ca^{2+} concentration (Feigenson, 1986). Although the Ca^{2+} binding and phase behavior of this three-component system are described by simple physical chemistry, a crucial increase in complexity would give the model much stronger predictive power for real biomembrane behavior: the PS concentration of the phospholipid bilayer should be varied over a wide range. Thus, the better model for Ca^{2+} binding between biomembranes is the four-component system of PS, phosphatidylcholine (PC), Ca^{2+}, and H_2O.

Some of the experimental difficulties posed by this PS/PC system were encountered before, and solved, with PS as the only lipid: analyzing Ca^{2+} binding between bilayers is easier if unilamellar lipid and hence interface without an apposed bilayer is minimized; Ca^{2+} must have access to the space between bilayers; and Ca^{2+} binding can be cooperative, thus equilibrium rather than supersaturation should be meausred (Feigenson, 1986). In addition, two difficulties not found with PS alone arise for PS/PC mixtures: (i) lipid phase separation can be induced by cooling, thus freeze–thawing should not be used to equilibrate Ca^{2+} across the bilayers; (ii) the product of Ca^{2+} binding is not readily separated from coexisting lipid without bound Ca^{2+}, so the chemical composition of the lipid phase that contains Ca^{2+} cannot be determined by chemical analysis, as was done for Ca^{2+} binding to PS without PC. We solve the problem of measuring an equilibrium Ca^{2+} concentration, without either forming additional unilamellar lipid or inducing spurious phase separation, with an approach used by Ohnishi and co-workers (Ohnishi & Ito, 1974; Tokutomi et al., 1979), by supporting the lipid multilayers in cellulose filters during both an initial Ca^{2+} binding period and a final Ca^{2+} dissolving period. We analyze the lipid phase that contains Ca^{2+} by indirect methods, by means of X-ray diffraction and ESR spectroscopy.

Experimental Procedures

Materials

Palmitoyloleoylphosphatidylserine (POPS) and palmitoyloleoylphosphatidylcholine (POPC) from Avanti Polar Lipids Inc. (Birmingham, AL) showed no impurities when 50 μg was chromatographed on Adsorbosil Plus P TLC plates with chloroform/methanol/concentrated NH_3, 25/10/2 v/v. Water was freshly purified through a Milli-Q system, and cellulose ester 5-μm filters were from Millipore Corp. (Bedford, MA). Chelex 100 ion-exchange resin from Bio-Rad (Rockville Center, NY) was cycled batchwise twice through 1 N HCl/1 N KOH. EGTA and Pipes buffer were of puriss grade from A. G. Fluka (Hauppauge, NY). $CaCO_3$ and HCl were of ultrex grade, and the phosphate standard was an analytical concentrate from J. T. Baker (Bricktown, NJ). The calcium chelator/indicators BAPTA and BrBAPTA were the tetrapotassium salts from Molecular Probes (Junction City, OR). Other chemicals were of reagent grade.

Methods

Preparation and Calibration of Solutions. All aqueous solutions contain 20 mM Pipes buffer and 100 mM KCl at pH 7.00. The buffer was stored in a polypropylene bottle over a bed of Chelex at 4 °C. Prior to use, the buffer was warmed to room temperature and then filtered through HCl-rinsed sintered glass to remove Chelex bead fragments.

† This work was supported by a grant from the National Institutes of Health, U.S. Public Health Service (HL-18255).

[1] Abbreviations: PS, 1,2-diacyl-*sn*-glycero-3-phosphoserine with specified or unspecified cations bound to neutralize charge; PC, 1,2-diacyl-*sn*-glycero-3-phosphatidylcholine; POPS, 1-palmitoyl-2-oleoyl-*sn*-glycero-3-phosphoserine; POPC, 1-palmitoyl-2-oleoyl-*sn*-glycero-3-phosphatidylcholine; BAPTA, 1,2-bis[bis(carboxymethyl)amino]ethane; BrBAPTA, 1,2-bis[[bis(carboxymethyl)amino](5-bromophenoxy)]-ethane; Pipes, piperazine-*N*,*N*′-bis(2-ethanesulfonic acid); EGTA, ethylene glycol bis(2-aminoethyl ether)-*N*,*N*,*N*′,*N*′-tetraacetic acid; A, sample absorbance; A_0, absorbance in the absence of Ca^{2+}; A_1, absorbance in excess Ca^{2+}; A', A divided by the absorbance at the isosbestic point (similarly for A_0' and A_1'); $[Ca^{2+}]^*$, characteristic aqueous Ca^{2+} concentration; S, order parameter; $\mathbf{a}_n$, thermodynamic activity of component n; γ, activity coefficient for PS in PS/PC mixture; γ', activity coefficient for Ca^{2+} in 20 mM Pipes and 100 mM KCl; v, variance; c, number of components; p, number of phases.

0006-2960/89/0428-1270$01.50/0

The primary standard Ca^{2+} solution and the solutions of EGTA, BAPTA, and BrBAPTA were prepared and titrated, and the concentrations of PS and PC in chloroform were determined as previously described (Feigenson, 1986).

Measurement of Ca^{2+} Concentration. Ca^{2+} chelators are used to establish free aqueous Ca^{2+} concentrations and, in the case of indicator dyes, to measure $[Ca^{2+}]$ [see, for example, Campbell (1983)]. We use a value of the dissociation constant K_D for Ca-EGTA in 20 mM Pipes and 100 mM KCl of 0.40 μM as the basis value for all Ca^{2+} determinations. This value for the Ca-EGTA dissociation constant is derived by pH correction and ionic strength interpolation from the measurements of K_D = 0.49 μM reported by Grynkiewicz et al. (1985) for Ca-EGTA binding at 18 °C, pH 7.02, in 225 mM KCl and 25 mM NaCl and K_D = 0.38 μM at 20 °C, pH 7.00, in 100 mM KCl. The K_D values for Ca-BAPTA and Ca-BrBAPTA under our conditions were determined, following the method of Tsien (1980), by finding the x-axis intercept of the plot of log $[(A - A_0)/(A_1 - A)]$ vs log $[Ca^{2+}]$. A_0 is the absorbance of the Ca^{2+}-free chelator, A_1 is the absorbance of the Ca^{2+}–chelator complex, and A is the absorbance of the chelator at a given $[Ca^{2+}]$, all at 253 nm for BAPTA and 262 nm for BrBAPTA. $[Ca^{2+}]$ was established by adding measured quantities of Ca^{2+} and EGTA, with [EGTA] 100-fold greater than [chelator]. This procedure gives the K_D for Ca-BAPTA as 0.24 μM and for Ca-BrBAPTA as 1.8 μM. Once the K_D is established, the concentration of free (uncomplexed) Ca^{2+} is found from

$$[Ca^{2+}] = K_D\frac{[\text{Ca–chelator}]}{[\text{free chelator}]} = K_D\left(\frac{A' - A_0}{A_1' - A'}\right) \quad (1)$$

where the prime indicates division of the measured absorbance at a peak in the difference spectrum by the measured absorbance at the isosbestic point. We find for BrBAPTA, A_0' = 1.49 and A_1' = 0.24 with absorbance measured at 262 nm and the isobestic point at 247.7 nm. For BAPTA, A_0' = 1.62 and A_1' = 0.16, with absorbance measured at 253 nm and the isosbestic point at 236.6 nm.

For all measurements of Ca^{2+} binding to PS/PC, samples of 100–150 μL were centrifuged in 250-μL polyethylene centrifuge tubes, which were supported in 2 M sorbitol and centrifuged at 13 000 rpm for 30 min in an SW-27 swinging bucket rotor at 20 °C. The pellet contained 99–100% of the lipid, as determined by phosphate analysis of the supernatant.

Ca^{2+} Equilibration Procedure. For a few of the experiments, a Ca^{2+}–chelator solution was added directly to a film of PS/PC, which had been dried under vacuum on the bottom of an acid-washed borosilicate culture tube. For most experiments, the PS/PC was supported in 5-μm pore size Millipore cellulose ester filters. The filters were washed five times with benzene over a one-week period in order to remove Triton X-100, followed by a wash with 50–100 μM BAPTA, and finally three washes with Milli-Q purified water. Pieces of these washed filters neither bound nor released Ca^{2+} (less than 5 μM) as determined from BAPTA absorbance. However, the filter pieces contribute to the measured absorbance at 236–262 nm and so require a correction, typically 1–2% of the absorbance.

The procedure for measuring Ca^{2+} binding began with addition of a chloroform solution of PS/PC to a small piece (typically 5 × 5 mm) of filter at the bottom of a polypropylene tube (12 × 75 mm). The sample was dried with N_2 followed by overnight mechanical pumping. Each filter containing PS/PC was then hydrated about 1 h in 100 μL of Pipes–KCl buffer under argon in the dark. Ca^{2+} was then added at defined free and total concentrations in order to control both the amount of binding and also the initial $[Ca^{2+}]$ at each PS/PC ratio. Thus, for PS/PC ratios of 1.00/0 to 0.5/0.5, Ca^{2+}/BAPTA was added at initial $[Ca^{2+}]$ of 0.4–6 μM and [BAPTA] of 80–500 μM; for PS/PC ratios of 0.5/0.5 to 0.30/0.7, Ca^{2+}/BrBAPTA was added at initial $[Ca^{2+}]$ of 6–24 μM and [BrBAPTA] of 100–400 μM; and for PS/PC ratios of 0.3/0.7 to 0.00/1.00, Ca^{2+} was added without chelator at initial $[Ca^{2+}]$ of 40–1000 μM. Tubes were sealed after flushing with argon and then rotated at 6–12 rpm in the dark in a water bath at 20 °C. After 1 week (unless the time course of binding was under study), aliquots of 100–150 μL were centrifuged. BAPTA was added to an aliquot of those supernatants having no chelator. The free and total Ca^{2+} concentrations were determined from the absorbance measurements, and the amount of Ca^{2+} bound was found from the difference between the initial and the final total Ca^{2+} concentrations.

The procedure for measuring the $[Ca^{2+}]$ that is in simultaneous equilibrium with lipid containing bound Ca^{2+} and PS/PC without bound Ca^{2+} began with removal of the lipid-containing filter from the Ca^{2+} binding medium after the aliquot had been withdrawn for binding measurement. The filter was gently blotted and then placed in a buffer of composition chosen to dissolve some of the lipid-bound Ca^{2+}. For PS/PC ratios of 1.00/0 to 0.5/0.5, [BAPTA] of 50–120 μM was used; for PS/PC ratios of 0.5/0.5 to 0.3/0.7 [BrBAPTA] of 50–80 μM was used; for PS/PC ratios of 0.3/0.7 to 0/1.00, buffer without chelator was used. Samples were sealed under argon and then slowly rotated in the dark at 20 °C for 2 weeks (unless the time course of dissolving Ca^{2+} was under study). Aliquots were then centrifuged, and absorbance was measured as above.

ESR. PS/PC samples on cellulose filter supports were prepared as described above for Ca^{2+} binding measurement. After 1 week of Ca^{2+} binding, one or two damp strips of lipid-containing filter, 4 × 15 mm, were placed on the outside flat walls of a quartz aqueous sample cell. Some samples were prepared by adding Ca^{2+} in buffer directly to a dry film of PS/PC on the bottom of a glass tube, slowly rotating the tube for one week, and then transferring the sample into the flat quartz cell. Spectra were recorded on a Varian E-4 X-band spectrometer with 100-kHz field modulation, interfaced to a PDP-11/23 computer.

X-ray Diffraction. PS/PC samples on filter supports were prepared as above. Four or five damp strips of lipid-containing filter, approximately 0.9 × 10 mm, were pushed to the bottom of a thin-walled glass capillary, 1-mm i.d. Diffraction measurements were made by use of the focused, monochromatic X-ray source at the Cornell High Energy Synchrotron Source (CHESS) as previously described (Caffrey, 1985).

Electron Microscopy. PS/PC samples on filter supports were fixed and stained in OsO_4 and then dried by mechanical pumping. The filter was embedded in Epon resin, sectioned, and poststained with lead citrate (Telford & Matsumura, 1970).

Visual Determination of Phase Boundaries. PS/PC mixtures in $CHCl_3$, approximately 60 mM in lipid, were added to 100.0-μL volumetric capillaries that had been sealed at one end. Samples of 2.5 μmol of total lipid were dried by mechanical pumping, with the vacuum gradually increased over 2 h, followed by pumping overnight. Buffer with or without Ca^{2+} or Ca^{2+}/BAPTA was added, and tubes were flushed with argon and then sealed. Tubes were centrifuged back and forth at approximately 200g, alternating with periods of incubation

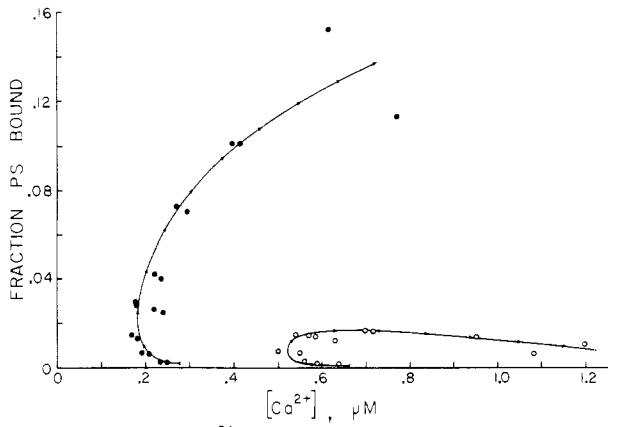

FIGURE 1: Binding of Ca^{2+} to POPS/POPC multilamellar liposomes shows supersaturation before binding begins, with only a small fraction of possible binding sites accessible. The arrowheads indicate increasing concentrations of Ca^{2+} added to POPS/POPC mixtures lyophilized from cyclohexane. Samples of 2 mM total lipid were slowly rotated at 20° for 5 days before $[Ca^{2+}]$ was measured. (●) POPS/POPC = 0.6/0.4; (○) POPS/POPC = 0.4/0.6.

at 20 °C, over 2 weeks. Each capillary was finally centrifuged at 13000 rpm for 4 h in an SW-27 swinging bucket rotor. The volumes of the lipid and aqueous phases were determined by linear measurement.

Results

We can attempt to examine the relationship of the extent of Ca^{2+} binding with the PS/PC ratio and the Ca^{2+} concentration by a direct approach: adding a Ca^{2+}-containing solution to a dry film of PS/PC, incubating the sample, and then measuring both the amount of Ca^{2+} bound and the final $[Ca^{2+}]$. This kind of experiment reveals the peculiar curves shown in Figure 1: a negligible amount of Ca^{2+} binds until a certain degree of supersaturation exists, whereupon Ca^{2+} binds. However, because of poor Ca^{2+} permeation through the hydrated lamellae, added Ca^{2+} increases the aqueous $[Ca^{2+}]$ after only little binding occurs.

In contrast, support of multilamellar samples on Millipore filters results in much more Ca^{2+} binding than occurs with liposomes. Samples of hydrated PS/PC, supported on washed cellulose Millipore filters, had the same appearance when observed by thin-section electron microscopy as did similar multilamellar preparations described by Tokutomi et al. (1979). Support of the samples also makes convenient the transfer of multilayers containing bound Ca^{2+} either to a sample holder for X-ray diffraction or ESR studies or else to a solution of Ca^{2+} chelator for the purpose of establishing an equilibrium $[Ca^{2+}]$. The time course of the $[Ca^{2+}]$ up to 120 h after addition of Ca^{2+}/BAPTA to hydrated PS/PC supported on Millipore filters is shown in Figure 2 for several different PS/PC ratios, each at two different initial $[Ca^{2+}]$ of $\approx$0.8 and $\approx$3 μM. Ca^{2+} binding does not increase significantly after four days. In order to dissolve a portion of the bound Ca^{2+} and thereby to determine an equilibrium $[Ca^{2+}]$ [see Feigenson (1986) for the rationale], the samples that had been exposed to aqueous Ca^{2+} for 120 h were transferred to buffer containing BAPTA. The time course of the $[Ca^{2+}]$ over a 96-h period is also shown in Figure 2: the $[Ca^{2+}]$ first drops as the chelator rapidly binds a small amount of accessible Ca^{2+} and then the $[Ca^{2+}]$ rises to approach an equilibrium value as bound Ca^{2+} dissolves. On the basis of these experiments, we chose standard incubation periods of 1 week for Ca^{2+} binding and 2 weeks for Ca^{2+} dissolving to reach an equilibrium value of $[Ca^{2+}]$. Lipid decomposition was found to be <1%, estimated from thin-layer chromatography in chloroform/methanol/water, 65/25/4, of 50-μg lipid samples that had been incubated for 5 weeks during $[Ca^{2+}]$ determinations.

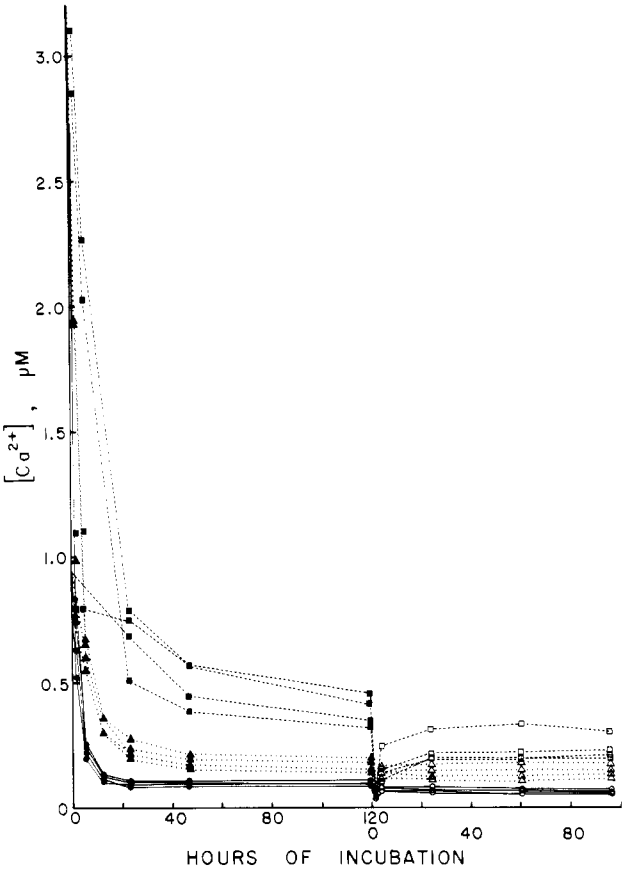

FIGURE 2: Time course of Ca^{2+} equilibration with POPS/POPC multilamellar samples supported on cellulose ester filters. The solid symbols show the time course of Ca^{2+} binding to POPS/POPC = 1.0/0 (●), 0.8/0.2 (▲), and 0.6/0.4 (■), each starting from initial $[Ca^{2+}]$ of 0.8 and 3 μM. After 120 h of incubation, samples were transferred to 0.05 mM BAPTA to reduce $[Ca^{2+}]$ below the equilibrium value. The open symbols show the time course of Ca^{2+} dissolving toward an equilibrium $[Ca^{2+}]$ for POPS/POPC = 1.0/0 (○), 0.8/0.2 (△), and 0.6/0.4 (□).

The dependence of the amount of Ca^{2+} bound on the equilibrium $[Ca^{2+}]$ is shown in Figure 3 for a range of PS/PC ratios. The data are plotted as the fraction of occupied sites vs the logarithm of the concentration of aqueous free Ca^{2+}. (Note that a logarithmic scale is used in order to fit the range of data on one graph, not to imply a relationship among parameters.) For each PS/PC ratio, added Ca^{2+} does not bind initially, but instead increases the aqueous free $[Ca^{2+}]$ *until a characteristic value of* $[Ca^{2+}]$ *is reached*, whereupon most of the added Ca^{2+} binds with little increase in the $[Ca^{2+}]$. Hereafter, we refer to this characteristic value of the aqueous free Ca^{2+} concentration when hydrated PS/PC, Ca^{2+}-bound lipid, and aqueous Ca^{2+} solution phases coexist as $[Ca^{2+}]^*$.[2]

[2] For pure POPS in 20 mM Pipes buffer and 100 mM KCl, extrapolation of the "fraction of PS bound" to zero gives $[Ca^{2+}]^* = 0.040 \pm 0.002$ μM. In earlier work with a buffer of 100 mM Pipes and 100 mM KCl, we found $[Ca^{2+}]^* = 0.14 \pm 0.05$ μM for POPS (Feigenson, 1986). Although the protocol used in the recent work allows binding to occur much closer to equilibrium and thus enables larger and more regular arrays of $Ca(PS)_2$ to form, there could be a real effect of ionic strength on the binding equilibrium. The filter support itself appears to have no effect on the binding strength since our most recent studies of Ca^{2+} binding to unsupported multilamellar POPS also give $[Ca^{2+}]^* = 0.04$ μM in the 20 mM Pipes and 100 mM KCl buffer (Joy Swanson, unpublished data). We note also that because the experiments shown in Figure 3 were designed to detect the onset of binding, data were obtained at low fractions of PS bound. At higher fractions of PS bound, the isotherms bend toward higher $[Ca^{2+}]$ (Feigenson, 1986, and data not shown).

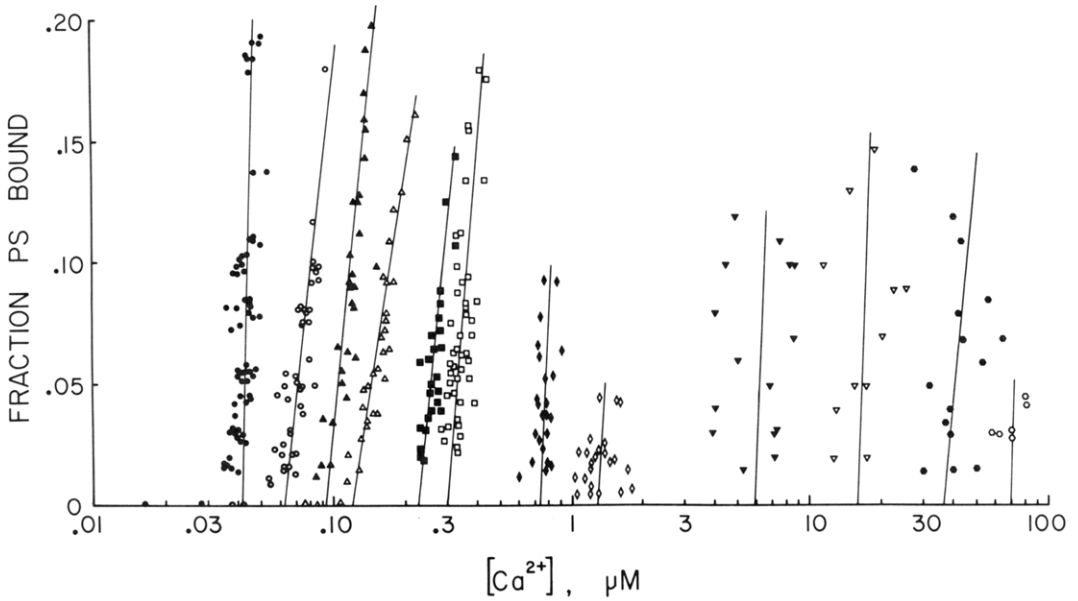

FIGURE 3: Ca^{2+} binding to multilamellar samples of POPS/POPC supported on cellulose ester filters. Samples were incubated in Ca^{2+}/chelator solutions for 1 week, during which time Ca^{2+} binding took place. Samples were then transferred to Ca^{2+}-free chelator solutions and incubated for 2 weeks, and the final $[Ca^{2+}]$ values shown in the figure were measured. POPS/POPC ratios are 1.0/0 (●), 0.8/0.2 (○), 0.7/0.3 (▲), 0.6/0.4 (△), 0.55/0.45 (■), 0.50/0.50 (□), 0.4/0.6 (◆), 0.3/0.7 (◇), 0.2/0.8 (▼), 0.15/0.85 (▽), 0.10/0.90 (⬢), and 0.05/0.95 (⬡). No Ca^{2+} binding to pure POPC was detected.

Table I: X-ray Diffraction Patterns of POPS/POPC Multilayers Containing Bound Ca^{2+}

mole ratio, PS/PC	lines obsd ($Å^{-1}$)	mole ratio, PS/PC	lines obsd ($Å^{-1}$)
1.0/0	49.1 and higher orders n = 2, 3, 5	0.4/0.6	49.1
	8.3		8.3
	4.8, 4.6, 4.5, 4.3, 4.2		4.8, 4.5
0.8/0.2	49.1 and higher orders n = 2, 3	0.2/0.8	49.1 and higher orders n = 2, 3
	8.3		8.3
	4.8, 4.5		4.8, 4.5, 4.2

For a given PS/PC ratio, the characteristic Ca^{2+} binding behavior is independent of the total lipid concentration over a range of 0.2–20 mM for PS/PC = 1.00/0 and 2–20 mM for PS/PC = 0.8/0.2 to 0.4/0.6. The total lipid concentration was fixed at 20 mM for PS/PC = 0.3/0.7 to 0/1.00. For pure palmitoyloleoyl-PC (without PS) at 20 mM, at the highest value of $[Ca^{2+}]$ examined, 1000 μM, one Ca^{2+} was bound per 2000 PC, a result that is near the measurement error. For comparison, Ca^{2+} binding to PS/PC = 0.05/0.95 was 5-fold greater than to pure PC.

Previous experiments have established by chemical analysis that Ca^{2+} binds to hydrated PS (without PC) to form $Ca_{1.00}(PS)_{2.00}$ (Feigenson, 1986). However, for PS/PC mixtures the nature of the Ca^{2+}-bound lipid must be determined by less direct methods because of the difficulty of physical separation of Ca^{2+}-bound lipid from coexisting lipid without bound Ca^{2+}. Thus, we compare the properties of pure $Ca(PS)_2$ with those of PS/PC containing bound Ca^{2+} by means of X-ray diffraction and ESR spectroscopy.

The X-ray diffraction patterns for filter-supported samples of PS/PC containing bound Ca^{2+} are given in Table I. Photographs of the diffraction patterns for PS/PC = 1.00/0 and 0.2/0.8 are shown in Figure 4. The same sharp features of the $Ca(PS)_2$ diffraction pattern are seen in the patterns for all ratios of PS/PC examined. In particular, the diffraction patterns show a series of sharp low-angle lines with Bragg spacings having the ratios $1:{}^1/_2:{}^1/_3$ etc., which correspond to a lamellar spacing of 49.1 Å; wide-angle lines at 4.5 $Å^{-1}$ and

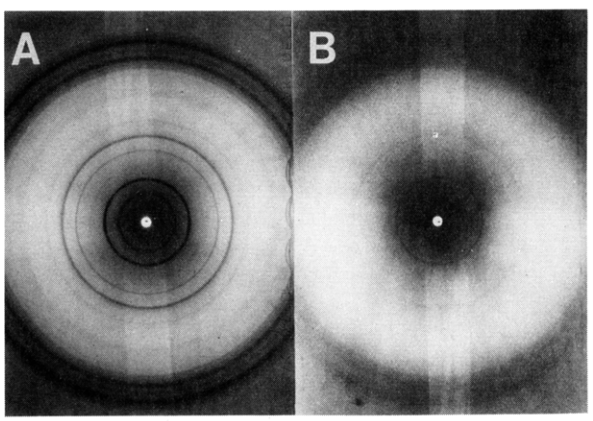

FIGURE 4: X-ray diffraction from multilamellar lipid samples recorded on X-ray sensitive film. (A) Pure POPS with $[Ca^{2+}]$ approximately 0.1 μM; 80–90% of the lipid is $Ca(PS)_2$, and the rest is hydrated PS. (B) POPS/POPC at an initial ratio of 0.2/0.8 with $[Ca^{2+}]$ approximately 0.6 mM; about 60% of the PS, or ~10% of the total lipid, is $Ca(PS)_2$, and the rest is hydrated PS/PC.

4.8 $Å^{-1}$ are observed, and a line at 8.3 $Å^{-1}$ that is characteristic of various Ca^{2+}-bound PS species (without PC) is apparent (Hauser & Shipley, 1984).

The possibility that Ca^{2+} binding to PS/PC mixtures leads to a rigid phase that contains no PC is addressed by ESR experiments with spin-labeled PS and spin-labeled PC. A simple experiment is to incorporate either (7,6)PS or (7,6)PC in POPS multilamellar liposomes and to record ESR spectra in the presence or absence of Ca^{2+}. The spectrum of (7,6)PS in POPS shows an increase in outer hyperfine splitting from 51 to 59 G (Figure 5A) caused by Ca^{2+} binding. This increase corresponds to a large change in the order parameter, from S = 0.55 to S = 0.8. In contrast, the spectrum of (7,6)PC in POPS shows only slight line broadening, with no change in hyperfine splitting, caused by Ca^{2+} binding (Figure 5B). The PS/PC samples on cellulose filters show behavior like that of the simple POPS liposomes: incubation of PS/PC = 0.5/0.5 containing (7,6)PS, with excess Ca^{2+} results in a new spectral component with outer hyperfine splitting of ~59 G (Figure

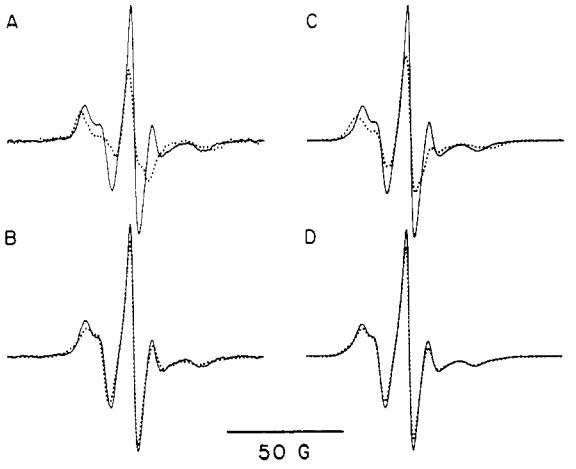

FIGURE 5: ESR spectra of spin-labeled lipids show immobilization of PS but not of PC upon addition of Ca^{2+} to multilamellar samples containing PS. Dotted lines show the presence of Ca^{2+} at 2 mM (A and B) or 10 mM (C and D) final concentration. (A) (7,6)PS/POPS = 1/1000; (B) (7,6)PC/POPS = 1/1000; (C) (7,6)PS/POPS/POPC = 0.005/0.495/0.500; (D) (7,6)PC/POPS/POPC = 0.005/0.500/0.495. Liposome dispersions (A and B) or filter-supported multilayers (C and D) were incubated with buffer for 1 week, and ESR spectra shown as solid lines were recorded. Ca^{2+} was then added, samples incubated for 2 weeks, and the ESR spectra shown as dotted lines were recorded.

Table II: Composition of Lipid Phase in the Presence of Excess Aqueous Phase

mole ratio, PS/PC	$[Ca^{2+}]$ (μM)	H_2O/total lipid, mole ratio at phase boundary
1.0/0	0	(200–250)/1
1.0/0	0.04	(175–225)/1
0.8/0.2	0	(200–250)/1
0.8/0.2	0.06	(225–275)/1
0.7/0.3	0	(200–250)/1
0.7/0.3	0.13	(200–250)/1
0.5/0.5	0	(175–225)/1
0.5/0.5	0.38	(175–225)/1
0.4/0.6	0	(250/300)/1
0.4/0.6	0.7	(250–300)/1
0.3/0.7	0	(175–225)/1
0.3/0.7	2	(175–225)/1
0.1/0.9	0	(175–225)/1
0.05/0.95	0	(125–175)/1
0/1.0	0	(40–45)/1
0/1.0	10^3	(50–55)/1
0/1.0	10^4	(55–60)/1
0/1.0	10^5	(40–45)/1

5C). In contrast, (7,6)PC incorporated in PS/PC = 0.5/0.5 shows no significant spectral changes after 2 weeks of incubation in excess Ca^{2+} (Figure 5D). Almost identical ESR results were observed for PS/PC = 0.6/0.4 and 0.4/0.6, showing no incorporation of (7,6)PC into a rigid phase under conditions where addition of Ca^{2+} causes pronounced ordering of (7,6)PS (data not shown).

In order to obtain additional phase information, PS/PC mixtures in capillary tubes were equilibrated with buffer with or without Ca^{2+}. From the known quantities of PS, PC, and water, together with the measured equilibrium volumes of the phases, the water/lipid ratio at the boundary of a two-phase region could be approximately determined. In these measurements the $[Ca^{2+}]$ was kept low enough that no significant binding to lipid occurred. Results are shown in Table II.

Discussion

Nature of the Ca^{2+} Binding Reaction. The stoichiometry of Ca^{2+} binding to pure PS lamellae was established in an earlier study (Feigenson, 1986) to be $Ca_{1.00}(PS)_{2.00}$ on the basis of binding isotherms showing no binding beyond this ratio as well as by chemical analysis of the binding product. For Ca^{2+} binding to PS/PC mixtures, we conclude that the chemical reaction is the same as that for pure PS because of three kinds of experimental results: (i) X-ray diffraction patterns (Table I and Figure 4) are consistent with the formation of an isomorphous product of Ca^{2+} binding to mixtures of PS/PC = 1.0/0, 0.8/0.2, 0.4/0.6, and 0.2/0.8; (ii) ESR spectra show that spin-labeled PS but *not* spin-labeled PC is found in the rigid lattice formed by Ca^{2+} binding to PS/PC mixtures (Figure 5); (iii) the fluorescent anthroyloxyl-labeled PC partitions out of $Ca(PS)_2$ and into coexisting fluid PS/PC with a partition coefficient of 100 favoring the fluid phase (Florine & Feigenson, 1987).

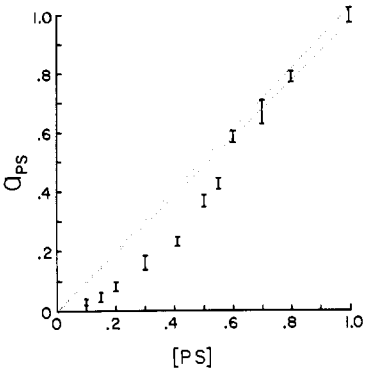

FIGURE 6: Nonideal mixing of POPS and POPC. The thermodynamic activity of the PS as given by $[(0.040\ \mu M\ Ca^{2+})/[Ca^{2+}]]^{1/2}$ (see text) is plotted against the mole fraction of PS. The dotted lines show the range of ideal mixing, given the experimental uncertainty of $[Ca^{2+}]^*$ for pure POPS of 0.040 ± 0.002 μM.

If we conclude that Ca^{2+} binds to PS/PC to form $Ca(PS)_2$, then an important relationship emerges between the value of the equilibrium calcium ion concentration, $[Ca^{2+}]$, and the PS concentration in the bilayer (data shown in Figure 3). The Ca^{2+} binding reaction is written as

$$Ca(PS)_2 + \text{water} \rightleftharpoons Ca^{2+}(aq) + 2PS^-(aq) \quad (2)$$

$$K_D = (a_{Ca^{2+}})(a^2_{PS^-})/a_{Ca(PS)_2} \quad (3)$$

The thermodynamic activity of a pure phase of $Ca(PS)_2$ is a constant, set at unity by choice of the standard state. The relationship between the thermodynamic activity and the measured concentration for Ca^{2+} in 20 mM Pipes and 100 mM KCl can be written as $a_{Ca^{2+}} = \gamma'[Ca^{2+}]$, where γ' is the activity coefficient for aqueous Ca^{2+}. The activity of PS can be expressed in terms of the PS mole fraction in the PS/PC bilayer as $a_{PS} = \gamma[PS]$. If we use the convention that $a_{PS} = 1$ when [PS] = 1, then from Figure 3 and eq 3 $K_D = \gamma'[Ca^{2+}]^* = \gamma'(0.040\ \mu M)$. For other values of PS/PC and $[Ca^{2+}]^*$

$$K_D/a_{Ca^{2+}} = 0.040\ \mu M/[Ca^{2+}]^* = a^2_{PS} = (\gamma[PS])^2 \quad (4)$$

A plot of a_{PS} vs [PS], i.e., $[(0.040\ \mu M)/[Ca^{2+}]^*]^{1/2}$ vs [PS], shown in Figure 6, reveals the nonideality of mixing of POPS in POPC. The behavior is familiar: PS follows Raoult's law at high PS concentration, consistent with ideal mixing of PS and PC; PS follows Henry's law at low PS concentration, with negative deviation from ideal mixing. For dilute PS, the slope yields an activity coefficient of ≈0.35. An activity coefficient less than unity in the Henry's law region is commonly observed for an attractive interaction between unlike molecules (Glasstone, 1946) as occurs, for example, for chloroform in acetone (von Zawidzki, 1900): hydrogen bonding occurs between unlike molecules. A different explanation is likely for dilute PS in PC: electrostatic repulsion between negatively

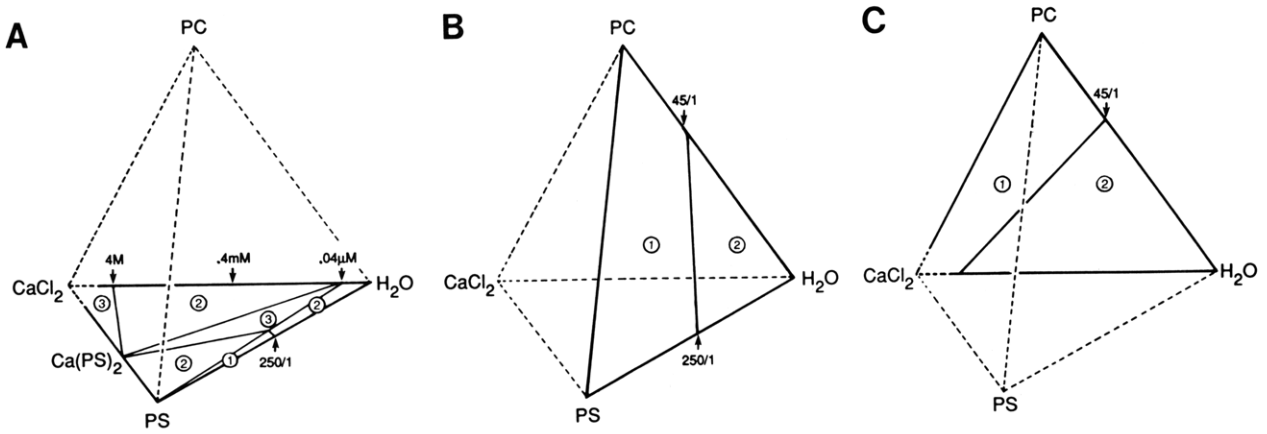

FIGURE 7: Pseudoquaternary phase diagram for PS, PC, Ca^{2+}, and water. Three-component regions at the faces of the tetrahedron are shown. Pressure is constant at 1 atm, temperature at 20 °C. The presence of Pipes buffer, KCl, and Ca^{2+} chelator is neglected. The diagram is not drawn to scale. The number of coexisting phases is shown as a circled number within a region. The regions of low water content are not explored, and this lack of information is emphasized by the broken lines that form the Ca^{2+} vertex. (A) The PS, Ca^{2+}, and water system [see Feigenson (1986) for a detailed discussion of this three-component system]. The one-phase hydrated PS region extends to $H_2O/PS = 250/1$. An aqueous Ca^{2+} concentration of 0.040 μM is in equilibrium with $Ca(PS)_2$ and hydrated PS in one three-phase region. In the other three-phase region saturated aqueous $CaCl_2$ of ~4 M is in equilibrium with solid hydrated $CaCl_2$ and $Ca(PS)_2$. The two-phase regions have coexisting $Ca(PS)_2$ + aqueous Ca^{2+}, $Ca(PS)_2$ + partially hydrated PS, and hydrated PS + aqueous Ca^{2+}. (B) The PS, PC, and water system is shown with two principal regions. The boundary is a line that intersects one edge at $H_2O/PC = 45/1$ and another edge at $H_2O/PS = 250/1$. (C) The PC, Ca^{2+}, and water system is shown with two principal regions. The boundary passes through $H_2O/PC \approx 45/1$ at $[Ca^{2+}] = 0$, 1, 10, and 100 mM.

charged PS molecules is relieved for PS–PC neighbors. Thus, the chemical potential of PS surrounded by PC is lower than that of PS surrounded by PS. If binding of K^+ ions to PS is neglected, then each PS probably has a full unit of negative charge at all values of the PS/PC ratio at pH 7 (MacDonald et al., 1976; Cevc et al., 1981; Tsui et al., 1986). Furthermore, among the factors that influence lipid mixing, the relative magnitude of an electrostatic repulsion would be large for POPS/POPC compared to any acyl chain effect. For lipid mixtures with differences in acyl chains, molecules with like acyl chains would tend to be neighbors.

The discussion above ascribes the observed dependence of the aqueous Ca^{2+} concentration on the PS/PC ratio at the phase boundary of $Ca(PS)_2$ formation to a molecular-level picture of the ideality of mixing PS and PC. However, two other categories of effects, in addition to PS/PC mixing, might influence the Ca^{2+} binding equilibrium: (i) a direct effect of Ca^{2+} or water on $\mathbf{a}_{PS}$ as a function of the PS/PC ratio; (ii) a variation in the free energy of bringing together lamellae of PS/PC via "bridges" of $Ca(PS)_2$ as a function of the PS/PC ratio.

The first effect (i) is likely to be small because the water/lipid ratio in the lipid phase does not vary significantly in the range PS/PC = 0.1/0.9 to 1.0/0 in the presence or absence of Ca^{2+} (Table I). Also, no binding of Ca^{2+} to fluid-phase PS/PC was detected, up to the boundary for $Ca(PS)_2$ formation. Thus, a direct influence of Ca^{2+} or of water on $\mathbf{a}_{PS}$ at the phase boundary for $Ca(PS)_2$ formation is unlikely.

The second effect (ii) refers to the possible dependence on the PS/PC ratio of the free energy to form bridges of $Ca(PS)_2$ between lamellae that are initially separated by 175–250 water molecules per lipid (80–110 Å between lamellae). This bridging might be influenced by a free energy required to distort the bilayer planarity or to partially dehydrate the fluid PS/PC. The effect might show up in the equilibrium value of $[Ca^{2+}]^*$ and/or in the nucleation (degree of Ca^{2+} supersaturation) for $Ca(PS)_2$ formation. We do not yet know how to estimate the importance of this effect.

Phase Diagrams. The Ca^{2+} binding isotherms of Figure 3 show that for every PS/PC mixture from 1.0/0 to 0.05/0.95

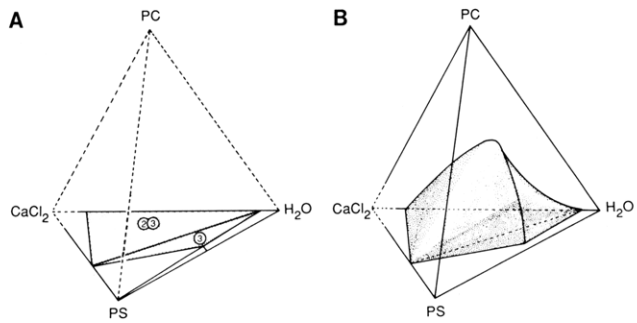

FIGURE 8: Three-phase volume region of the tetrahedron pictured as arising from areas of the PS, Ca^{2+}, water system upon addition of PC. (A) The two-phase area of $Ca(PS)_2$ + aqueous Ca^{2+} must accommodate some PC, although the amount of PC either in $Ca(PS)_2$ or in the aqueous phase has been too small to measure. Thus, the diagram indicates where a thin, two-phase volume must form, underlying a three-phase area of coexisting $Ca(PS)_2$ + hydrated PS containing a trace of PC + aqueous Ca^{2+}. This three-phase area is continuous with the three-phase area shown in the face of the tetrahedron that contains no PC. (B) The three-phase areas shown in (A) become a three-phase volume as PC concentration increases. At any point within this volume coexist $Ca(PS)_2$, fully hydrated PS/PC, and aqueous Ca^{2+}.

added Ca^{2+} does not bind (i.e., is no more concentrated in the lipid phase that in the aqueous phase) until a particular Ca^{2+} concentration ($[Ca^{2+}]^*$) is reached that is characteristic of the value of PS/PC. Once binding begins, the $[Ca^{2+}]^*$ is essentially invariant. There is no dependence of this characteristic $[Ca^{2+}]^*$ on the amount of $Ca(PS)_2$ formed or on the amount of the PS/PC mixture that is present initially. This independence of thermodynamic activity as the amount of a substance varies is the hallmark of a pure phase. Thus, both $Ca(PS)_2$ and hydrated PS/PC behave as pure phases when both are coexisting with an aqueous Ca^{2+} phase. This conclusion enables us to apply the phase rule (Findlay, 1951): $v = c - p + 2$, where v is the variance of the system, c is the number of components, and p is the number of phases. In our study, $c = 4$ (PS, PC, Ca^{2+}, and H_2O are capable of independent concentration changes). Temperature and pressure are fixed at 20 °C and 1 atm. When three phases coexist, the variance must be one. Indeed, we observe that the PS/PC

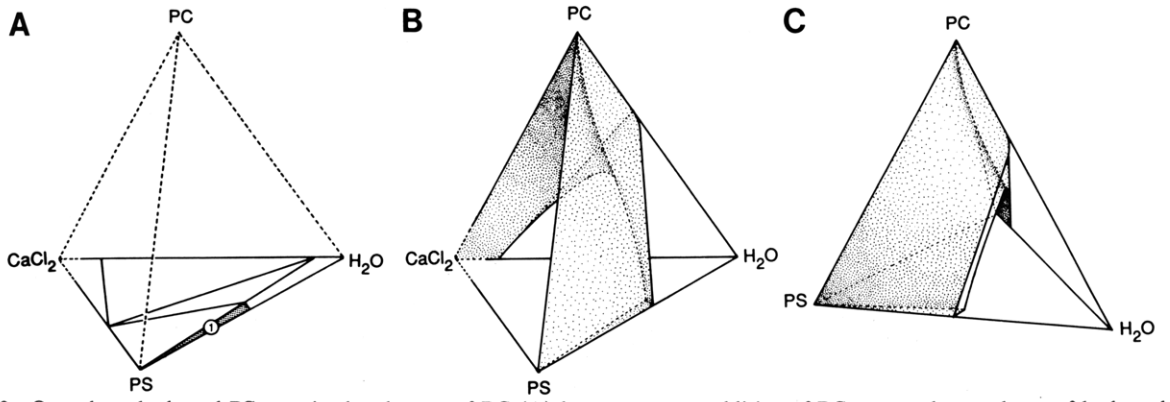

FIGURE 9: One-phase hydrated PS area in the absence of PC (A) becomes, upon addition of PC, a one-phase volume of hydrated PS/PC, shown in two views, (B) and (C). The amount of Ca^{2+} added is too small for high-affinity binding at any given PS/PC ratio within the one-phase volume. Thus, the concentration of Ca^{2+} in this phase ranges from zero up to the concentration at which $Ca(PS)_2$ forms.

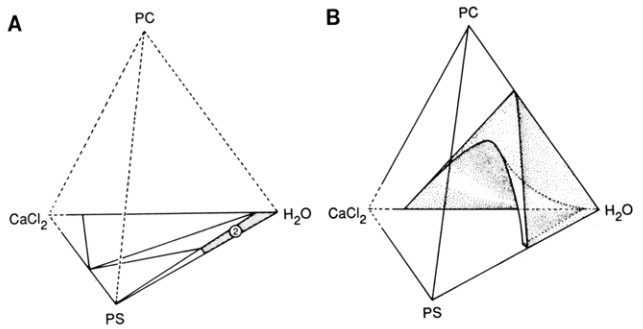

FIGURE 10: Two-phase hydrated PS area in the absence of PC (A) becomes, upon addition of PC, a two-phase volume of hydrated PS/PC + aqueous Ca^{2+} (B). The amount of Ca^{2+} added is too small for high-affinity binding at any given PS/PC ratio within the two-phase volume.

composition can be varied (i.e., "chosen"), and thereupon the concentration $[Ca^{2+}]^*$ is fixed. This discovery of a characteristic Ca^{2+} concentration $[Ca^{2+}]^*$ that is invariant for a given PS/PC ratio when $Ca(PS)_2$, hydrated PS/PC, and aqueous Ca^{2+} coexist at equilibrium implies the absence of any essential importance in the product of the aqueous $[Ca^{2+}]$ with the amount of PS or in the ratio of bound Ca^{2+} to the amount of PS.

These observations of the phase behavior of PS, PC, Ca^{2+}, and water are organized in a pseudoquaternary phase diagram that is shown in the series of Figures 7–11. This diagram contains likely, but unexplored, regions (Figure 11) in order to complete the description: samples of low water content and/or $[Ca^{2+}]$ greater than 100 mM were not studied. The presence of components, namely, Pipes buffer, KCl, and Ca^{2+} chelator, in addition to those at the vertices of the tetrahedron, is neglected. This diagram is based upon the following observations: (i) a pure phase of $Ca(PS)_2$ can form; (ii) when $Ca(PS)_2$ and hydrated PS/PC coexist, the aqueous Ca^{2+} concentration is fixed at a value $[Ca^{2+}]^*$ characteristic of the ratio of PS/PC found at equilibrium; (iii) $[Ca^{2+}]^*$ is independent of the total lipid concentration; (iv) for $[Ca^{2+}] < [Ca^{2+}]^*$, a hydrated PS/PC phase and an aqueous phase coexist, with virtually the same $[Ca^{2+}]$ in each phase; (v) PS/PC lamellae take up water and exist as a single phase until water is in excess; (vi) the aqueous phase contains very little PS or PC; (vii) $CaCl_2$ has limited solubility in water, precipitating as a hydrated solid at low water concentration.

In order to show clearly the regions of interest, Figures 7–11 are not drawn to scale. The range of Ca^{2+} concentrations studied, ~0.02 μM–100 mM, is shown on a diagram that extends from pure $CaCl_2$ to pure water. The stoichiometry of the $Ca(PS)_2$ phase is correctly scaled on a mole fraction basis between pure PS and pure $CaCl_2$.

Figures 8–11 each show particular *areas* of the PS, Ca^{2+}, water system, together with four-component *volumes*, in order to clarify the relationship between the three-component area region and a volume region of the four-component PS, PC, Ca^{2+}, water system.

Finally, we emphasize that the regions of low water content and/or high Ca^{2+} concentration are likely to have complex phase behavior, which is not shown on the diagram.

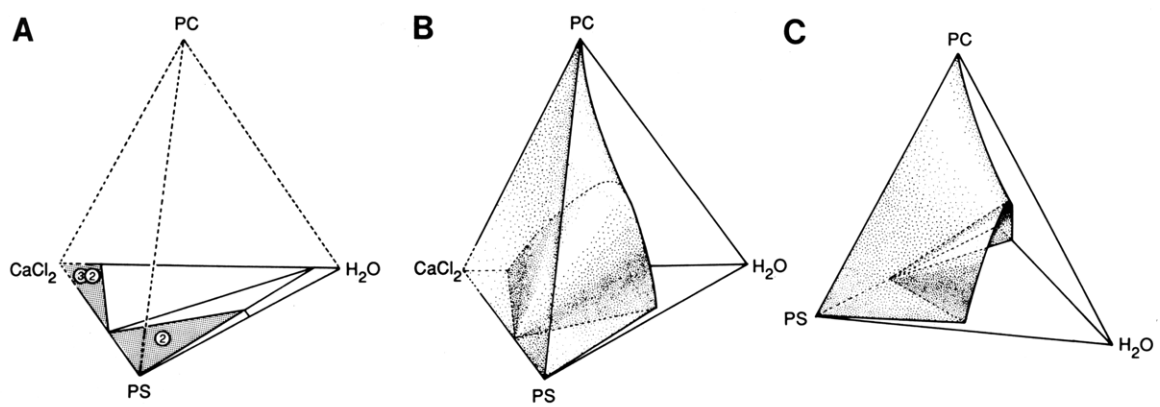

FIGURE 11: Two-phase volume region of low water content pictured as arising from two-phase areas of the PS, Ca^{2+}, H_2O system upon addition of PC. (A) An unexplored but likely region of the diagram has three coexisting phases: $Ca(PS)_2$, solid hydrated $CaCl_2$, and saturated aqueous $CaCl_2$. When the total concentration of Ca^{2+} decreases and the concentration of PC increases sufficiently, both the solid hydrated $CaCl_2$ phase and the saturated aqueous $CaCl_2$ phase must disappear, eventually leaving two phases: $Ca(PS)_2$ and partially hydrated PS/PC/Ca^{2+}. The boundary of this two-phase region is not determined but is indicated schematically as overlying a three-phase area. Also shown in (A) is a two-phase area in the plane of the PS, Ca^{2+}, water system, from which the two-phase volume region can be pictured as arising upon addition of PC, as shown in two views, (B) and (C).

We can understand the shape of the Ca^{2+} binding isotherms shown in Figure 3 by referring to the phase diagram: A sample at the start of each isotherm corresponds to a point in the two-phase area of Figure 7B, established by the PS/PC ratio and the total lipid/water ratio. Adding Ca^{2+} to this sample corresponds to moving from this point toward the Ca^{2+} vertex. High-affinity Ca^{2+} binding begins at the intersection of the volume shown in Figure 8B. At this boundary $Ca(PS)_2$ forms, in equilibrium with hydrated PS/PC at the initial ratio and the aqueous Ca^{2+} concentration $[Ca^{2+}]^*$ that is characteristic of this PS/PC ratio (see eq 4). As more Ca^{2+} is added, more $Ca(PS)_2$ forms, the ratio of PS/PC in the coexisting hydrated lipid phase decreases, and the equilibrium $[Ca^{2+}]$ increases. These changes in composition of coexisting PS/PC and $[Ca^{2+}]$ as Ca^{2+} is added correspond to the small positive slope of the isotherms in Figure 3.

Comparison with Unilamellar Vesicle Studies. In both this and an earlier study (Feigenson, 1986) we observed supersaturation of aqueous Ca^{2+} prior to the onset of high-affinity binding. Because we choose to use an equilibrium thermodynamic approach, we overcome supersaturation (essentially by incubating samples for weeks and by partially dissolving the Ca^{2+}-bound lipid). High-affinity Ca^{2+} binding between unilamellar vesicles would also be subject to supersaturation; i.e., there is a significant free energy barrier to nucleate Ca^{2+} lipid-phase formation. The cation concentration required to nucleate a phase in model studies has little predictive value because it would not be directly related to a biological phenomenon wherein a nucleation barrier could be subject to control, or at least could be strongly dependent upon other components. In contrast, because there exist well-defined relationships among the *equilibrium* values of component thermodynamic activities, the phase behavior and the chemical equilibria that underlie the observed Ca^{2+} binding between bilayers are revealed.

Why Is $Ca(PS)_2$ So Stable? A reasonable but qualitative explanation for $Ca(PS)_2$ stability (i.e., for high-affinity Ca^{2+} binding to PS) emphasizes the observation that the binding of aqueous Ca^{2+} to the hydrated PS surface *without an apposed bilayer is low-affinity binding*, about 6 orders of magnitude weaker than the binding between lamellae (Nir et al., 1978; McLaughlin et al., 1981). The apposed bilayers are capable of strong mutual attraction (Guldbrand et al., 1984; Kjellander & Marcelja, 1985; Marra, 1986; Rand et al., 1988). Because $Ca(PS)_2$ is a chemically well-defined compound, the nature of its stability cannot lie in correlated fluctuations that require chemical variation. Instead, the stability of $Ca(PS)_2$ (relative to that of hydrated Ca^{2+} and hydrated PS/PC lamellae) is probably derived from (i) the *chelation* of Ca^{2+} by six to eight well-disposed PS headgroup ligands, together with the favorable enthalpy of Ca^{2+} binding to carboxyl and/or phosphate moieties; (ii) an orderly array of Ca^{2+}–phosphoserine that completely eliminates electrostatic and hydration repulsive forces (Ohki, 1984; Marra, 1986); and (iii) a large attractive dispersion interaction at close approach (Ninham & Parsegian, 1970). These attractive interactions are not manifested by individual PS molecules, but instead require locally cooperative PS conformations together with the large numbers of PS molecules necessary for interlamellar interactions. Thus, there is a phase transition.

Significance. POPS and POPC are chemically well-defined, yet reasonably representative of naturally occurring phospholipids. Ca^{2+} binds with high affinity between bilayers of these lipids in a range of POPS/POPC ratios and aqueous Ca^{2+} concentrations that occur in biological systems. For example, at POPS/POPC = 0.2/0.8, Ca^{2+} binds with high affinity at $[Ca^{2+}] \approx 6$ μM. Because the formation of the Ca^{2+}-bound phase of $Ca(PS)_2$ requires virtual contact of two bilayers, the biological phenomenon of Ca^{2+}-dependent membrane fusion might involve a phase transition of the sort described here.

Acknowledgments

I am grateful for the help of a number of people: M. Caffrey performed the X-ray diffraction measurements; J. Telford obtained the electron micrographs; H. Tann created a computer graphics representation and W. Pires drew the phase diagrams used in the figures; T. Kato and T. Ito clarified the interpretation of PS/PC nonideal mixing; S. McLaughlin pointed out that K^+ binding to PS would be significant; W. White and R. Kay increased my understanding of quaternary phase diagrams; M. Yeager participated in many helpful discussions; and K. Reiss and E. Patterson typed the manuscript.

Registry No. POPS, 40290-44-6; POPC, 26853-31-6; Ca, 7440-70-2.

References

Caffrey, M. (1985) *Biochemistry 24*, 4826–4844.
Campbell, A. K. (1983) *Intracellular Calcium*, Wiley, Chichester, U.K.
Cevc, G., Watts, A., & Marsh, D. (1981) *Biochemistry 20*, 4955–4965.
Ekerdt, R., & Papahadjopoulos, D. (1982) *Proc. Natl. Acad. Sci. U.S.A. 79*, 2273–2277.
Ekerdt, R., Dahl, G., & Gratzl, M. (1981) *Biochim. Biophys. Acta 646*, 10–22.
Feigenson, G. W. (1986) *Biochemistry 25*, 5819–5825.
Findlay, A. (1951) *The Phase Rule* (Campbell, A. N., & Smith, N. O., Eds.) 9th ed., pp 7–19, 277–182, Dover, New York.
Florine, K. I., & Feigenson, G. W. (1987) *Biochemistry 26*, 1757–1768.
Glasstone, S. (1946) *Physical Chemistry*, 2nd ed., pp 677–678, 711–713, Van Nostrand, Toronto.
Grynkiewicz, G., Poenie, M., & Tsien, R. Y. (1985) *J. Biol. Chem. 260*, 3440–3450.
Guldbrand, L., Jönsson, B., Wennerström, H., & Linse, P. (1984) *J. Chem. Phys. 80*, 2221–2228.
Hauser, H., & Shipley, G. G. (1984) *Biochemistry 23*, 34–41.
Kjellander, R., & Marcelja, S. (1985) *Chem. Scr. 25*, 112–116.
Koter, M., deKruijff, B., & van Deenen, L. L. M. (1978) *Biochim. Biophys. Acta 514*, 255–263.
Leventis, R., Gagnē, J., Fuller, N., Rand, R. P., & Silvius, J. R. (1986) *Biochemistry 25*, 6978–6987.
Liao, M. J., & Prestegard, J. H. (1980) *Biochim. Biophys. Acta 601*, 453–461.
MacDonald, R. C., Simon, S. A., & Baer, E. (1976) *Biochemistry 15*, 885–891.
Marra, J. (1986) *Biophys. J. 50*, 815–825.
McLaughlin, S., Mulrine, N., Gresalfi, T., Vaio, G., & McLaughlin, A. (1981) *J. Gen. Physiol. 77*, 445–473.
Morris, S. J., Costello, M. J., Robertson, J. D., Südhof, T. C., Odenwald, W. F., & Haynes, D. H. (1983) *J. Auton. Nerv. Syst. 7*, 19–23.
Ninham, B. W., & Parsegian, V. A. (1970) *J. Chem. Phys. 52*, 4578–4587.
Nir, S., Newton, C., & Papahadjopoulos, D. (1978) *Bioelectrochem. Bioenerg. 5*, 116–133.

Nir, S., Bentz, J., Wilschut, J., & Düzgünes, N. (1983) *Prog. Surf. Sci. 13*, 1–124.
Ohki, S. (1984) *J. Membr. Biol. 77*, 265–275.
Ohnishi, S.-I., & Ito, T. (1974) *Biochemistry 13*, 881–887.
Portis, A., Newton, C., Pangborn, W., & Papahadjopoulos, D. (1979) *Biochemistry 18*, 780–789.
Rand, R. P., Fuller, N., Parsegian, V. A., & Rau, D. C. (1988) *Biochemistry 27*, 7711–7722.
Telford, J. N., & Matsumara, F. (1970) *J. Econ. Entomol. 63*, 795–800.
Tokutomi, S., Eguchi, G., & Ohnishi, S.-I. (1979) *Biochim. Biophys. Acta 552*, 78–88.
Tsien, R. Y. (1980) *Biochemistry 19*, 2396–2404.
Tsui, F. C., Ojcius, D. M., & Hubbell, W. L. (1986) *Biophys. J. 49*, 459–468.
von Zawidzki, J. (1900) *Z. Phys. Chem. 35*, 129–203.

Isotopic Labeling Affects 1,25-Dihydroxyvitamin D Metabolism†

Bernard P. Halloran,* Daniel D. Bikle, Margaret E. Castro, and Elaine Gee
Departments of Medicine and Physiology, University of California, and Division of Endocrinology, Veterans Administration Medical Center, San Francisco, California 94121

Received June 2, 1988; Revised Manuscript Received September 21, 1988

ABSTRACT: Isotope substitution can change the biochemical properties of vitamin D. To determine the effect of substituting ^3H for ^1H on the metabolism of $1,25(OH)_2D_3$, we measured the metabolic clearance rate and renal metabolism of unlabeled and ^3H-labeled $1,25(OH)_2D_3$. Substitution of ^3H for ^1H on carbons 26 and 27 [$1,25(OH)_2[26,27(n)\text{-}^3H]D_3$] or on carbons 23 and 24 [$1,25(OH)_2[23,24(n)\text{-}^3H]D_3$] reduced the in vivo metabolic clearance rate of $1,25(OH)_2D_3$ by 36% and 37%, respectively, and reduced the in vitro renal catabolism of $1,25(OH)_2D_3$ by 11% and 54%, respectively. Substitutions of ^3H for ^1H on carbons 23 and 24 as opposed to carbons 26 and 27 reduced conversion of [^3H]$1,25(OH)_2D_3$ to [^3H]$1,24,25(OH)_2D_3$ by 25% and to putative 24-oxo-1,23,25-dihydroxyvitamin D_3 by 1600%. These results indicate that substitution of ^3H for ^1H on carbons 26 and 27 or on carbons 23 and 24 can reduce the metabolic clearance rate and in vitro metabolism of $1,25(OH)_2D_3$ and quantitatively alter the pattern of metabolic products produced.

Isotopically labeled vitamin D and metabolites of vitamin D are used extensively in studies of vitamin D metabolism. These studies have proven to be extremely valuable in defining how vitamin D is metabolized and in isolating the biologically active forms of the vitamin. In most cases, it is tacitly assumed that substitution of ^3H or ^2H for ^1H or ^{14}C for ^{12}C has little, if any, effect on the physicochemical or biochemical properties of the molecules. However, isotopic labeling can alter the chromatographic properties of many molecules, including the vitamin D metabolites (Blake et al., 1975; deRidder & van Hall, 1976; Oats et al., 1978; Horning et al., 1979; Thenot et al., 1980; Halloran et al., 1984). We have shown, for example, that substitution of ^3H for ^1H on carbon 23 (C-23) and carbon 24 (C-24) can change the retention times of 1,25-dihydroxyvitamin D_3 [$1,25(OH)_2D_3$][1] and 25,26-dihydroxyvitamin D_3 [$25,26(OH)_2D_3$] on silica columns by as much as 3.7% (Halloran et al., 1984).

Isotopic labeling can also alter metabolic properties and, in particular, the metabolism of vitamin D (Elison et al., 1961; Horning & Lertratanangkoon, 1978; Jones et al., 1983; Tanaka & DeLuca, 1982; Bell et al., 1986; Langenhove, 1986). Although there are no direct studies comparing the metabolic properties of labeled and unlabeled vitamin D, Tanaka and DeLuca (1982) showed that substitution of ^3H for ^1H in 25-hydroxyvitamin D (25-OH-D) can alter its metabolism in vitro. These investigators report that the in vitro rate of metabolic conversion of [^3H]-25-OH-D_3 to [^3H]-24,25-dihydroxyvitamin D_3 [[^3H]$24,25(OH)_2D_3$] or [^3H]$25,26(OH)_2D_3$ is dependent upon where the ^3H is incorporated into 25-OH-D_3 (Tanaka & DeLuca, 1982). Conversion of [^3H]-25-OH-D_3 to [^3H]-$24,25(OH)_2D_3$ is favored when [^3H]-25-OH-D_3 is labeled in the C-26 and -27 positions, whereas conversion to [^3H]-$25,26(OH)_2D_3$ is favored when the [^3H]-25-OH-D_3 is labeled in the C-23 and -24 positions. No study, however, has addressed the effect of ^3H-labeling on the metabolism of $1,25(OH)_2D$, the most biologically active form of vitamin D.

To determine whether substitution of ^3H for ^1H on C-23 and -24 or on C-26 and -27 changes the metabolism of $1,25(OH)_2D_3$, we examined the in vivo metabolic clearance rate (MCR) and in vitro renal metabolism of $1,25(OH)_2D_3$, $1,25(OH)_2[26,27(n)\text{-}^3H]D_3$, and $1,25(OH)_2[23,24(n)\text{-}^3H]D_3$. Our results indicate that ^3H-labeling can reduce the metabolism of $1,25(OH)_2D$ in vivo and in vitro and change the profile of metabolites produced.

Materials and Methods

Animals. Male Sprague-Dawley rats (Bantin and Kingman, Fremont, CA) weighing 100–125 g were fed ad libitum a semipurified, vitamin D deficient diet containing 1.2% calcium and 0.9% phosphorus (Suda et al., 1970). All rats were supplemented with vitamin D_3 (200 IU/day) and maintained on their diet for at least 10 days before experimentation.

Metabolic Clearance Rate. The metabolic clearance rate (MCR) was measured by using the constant infusion method as previously described (Halloran et al., 1986). Rats were

† This work was supported by the Veterans Administration Research Service.
* Address correspondence to this author at Veterans Administration Medical Center, m/c 11, 4150 Clement St., San Francisco, CA 94121.

[1] Abbreviations: 25-OH-D_3, 25-hydroxyvitamin D_3; $1,25(OH)_2D_3$, 1,25-dihydroxyvitamin D_3; $24,25(OH)_2D_3$, 24,25-dihydroxyvitamin D_3; $25,26(OH)_2D_3$, 25,26-dihydroxyvitamin D_3; 24-oxo-$1,23,25(OH)_3D_3$, 24-oxo-1,23,25-trihydroxyvitamin D_3.